

# Experimental research on impulse coupling effect of a multi-pulse laser on an aluminum target

Qianqian Shi (石乾乾)<sup>1,\*</sup>, Yan Zhang (张艳)<sup>2,\*\*</sup>, Kunpeng Wang (王鲲鹏)<sup>1</sup>,  
Chenglin Wang (王成林)<sup>1</sup>, and Peng Zhao (赵鹏)<sup>1</sup>

<sup>1</sup>Beijing Institute of Tracking and Telecommunications Technology, Beijing 100094, China

<sup>2</sup>School of Aeronautics and Astronautics, Sun Yat-sen University, Guangzhou 510275, China

\*Corresponding author: qiansnow@163.com; \*\*corresponding author: zhyan1227@sina.com

Received August 17, 2018; accepted October 24, 2018; posted online November 27, 2018

Impact and torsion pendulums are applied in impulse coupling experiments of high-energy laser irradiation of space debris. It is difficult to achieve a multi-pulse experiment and thus hard to analyze the multi-pulse impulse coupling effect. Here, we designed a new recoil impulse experimental measurement system of non-contact, multi-degrees of freedom, and multi-pulse irradiation. The system used a low-pressure and low-temperature vacuum chamber to simulate the space environment, the pinning effect of magnetic levitation to achieve aluminum target suspension, and high-speed cameras to record the displacement over time to calculate the impulse of the target. Then the impulse coupling experiment of multi-pulse laser irradiation on the aluminum target was performed. The result shows that the multi-pulse impulse coupling effect is not the linear accumulation of coupling results by every single-pulse and multi-pulse coefficient that decreases with the increase of the number of pulses, and eventually stabilizes as the decrease gets smaller.

OCIS codes: 140.3325, 140.3390, 140.3538.

doi: 10.3788/COL201816.121401.

Pollution of the space environment is getting more and more serious due to space debris, especially those of centimeters in size. Active clearance of centimeter space debris is the inevitable choice and the only way out<sup>[1-5]</sup>. At present, the active removal of space debris using high-energy lasers has become an internationally accepted method<sup>[6-10]</sup>. High-energy laser irradiation of space debris generates plasma plumes, and the space debris is dropped into the atmosphere by the recoil impulse caused by the plasma plume back injection, and then burned up to achieve the removal. In the 21st century, the United States, Germany, Japan, and China have successfully developed high-energy laser technology<sup>[11-14]</sup>, research of impulse coupling characteristics of laser-mass interaction<sup>[15-19]</sup>, a space debris orbital dynamic model, and other related technologies<sup>[20,21]</sup>. In particular, they have conducted a large number of basic experimental studies on the impulse coupling characteristics of laser irradiation on space debris, and the experimental research mainly focuses on the measurement and calculation of the impulse coupling coefficient. Most of the experiments use impact pendulums and torsion pendulums to carry out recoil impulse measurements, some use horizontal two-line guide rails, and a small number of experiments use pressure sensors<sup>[22]</sup>. The current experimental measuring devices have to touch the target to carry out the measurements, i.e., damping exists and affects the measurement result. In addition, measuring devices have an insufficient capability of multi-pulse impulse coupling; that is, they can only measure the impulse coupling coefficient after a single-pulse action. We are more concerned with the overall effect of space debris impinged on by a series of laser

pulses, but it is difficult to study the impulse coupling effect of multi-pulse laser irradiation on space debris.

In this Letter, we designed a non-contact, multiple-degrees-of-freedom experimental system that can measure recoil impulses to overcome those drawbacks. The experimental devices in this Letter mainly are comprised of a vacuum test chamber, a superconducting magnetic levitation system, a displacement measurement system, and a high-energy laser. As the core parts of our experimental system, the chamber and the maglev system can create the low temperature, low pressure, and weightless space environment for the aluminum target, and the structural design is shown in Fig. 1. The laser emits a high-energy pulsed beam toward the aluminum target to couple with it to generate the recoil impulse. The displacement

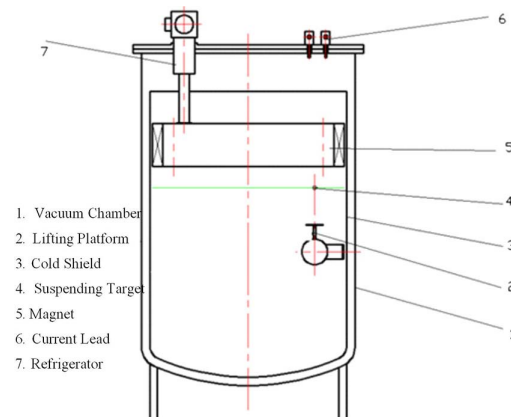


Fig. 1. Structural design for the vacuum chamber and maglev system.

measurement system obtains the displacement of the target by two cameras under the conditions of no contact and no damping. The photo of our experimental devices is shown in Fig. 2.

The vacuum test chamber is a vertical container with an inner diameter of 1000 mm and a straight section length of 1250 mm. Three circular observation windows are equipped outside the container. The middle observation window is a fully transparent lens, and the high-energy laser passes through it. This window can be opened for easy pick-and-place of the target. The observation windows on both sides are high-pressure lenses for the cameras that are capturing and recording images. As shown in Fig. 1, a lifting platform with the functions of cooling and heating is designed to hold the target. The platform has two degrees of freedom along the vertical direction and the radial direction of the container, and both movement strokes are 100 mm. The vertical freedom is achieved by means of a manual drive, which is a hand wheel set below the middle observation window. The vacuum test chamber uses a high-vacuum air pumping system with two molecular pumps as the main pumps and has no steam pollution and no electromagnetic interference.

The magnetic levitation system is mainly used for simulating the microgravity or weightless environments in space. Magnetic levitation is achieved by utilizing the pinning effect of a superconductor in a magnetic field. A racetrack-shaped NbTi electromagnetic coil and a high-temperature superconductor YBCO (yttrium barium copper oxide compound) together constitute the magnetic levitation system. The electromagnetic coil (the magnet) can generate a magnetic field distribution with enough field strength and uniformity in the target region. The pinning effect happens when the temperature of the superconductor falls below the critical temperature (about 90 K), which means that it undergoes a transition from a normal-conducting state to a superconducting state (referred to as field cooling) in the magnetic field. The YBCO superconductor will be locked in the uniform magnetic field as its levitation force counteracts the gravity. The lower the temperature drops, the stronger the suspension stiffness and stability are. Therefore, only

the horizontal motion can be performed and there is no damping in the direction that can be considered as “free motion” horizontally. Below the magnet, a “free” movement district with a suspension height of 5–10 cm and a length of 50 cm can be formed.

The displacement measurement system uses the camera measurement method. It is a non-contact measurement method that is intuitive, automated, and highly accurate, and is very suitable for monitoring the target’s parameters of displacement and attitude. Two digital cameras capture the suspending target from two directions and performs real-time or post-processing analysis on the collected sequence image to calculate the position parameters of the suspending target relative to the world coordinate system. The target to be measured is abstracted as a mass point, and the light is used to make the target display more prominent features than the background. For example, the background is set to a dark color and the mass point is set to a bright color. As long as the target has a little obvious feature point, the high-speed cameras can easily identify and track the target and measure its position information. In this experiment, the center of the spherical object can reflect a distinct bright spot, which we use as a feature point. In this way, particle features can be extracted from the image by simple segmentation. The principle of two camera measurements is that the position of the cameras is known and the cameras can obtain the angle information of target. According to the cameras’ position information and the target’s angle information, the absolute position of the target in space can be determined.

The high-energy laser system used in our experiment can generate the required pulse with a wavelength of 1064 nm, a pulse width of 10 ns, and a beam diameter of 1.2 cm. It also has an adjustable energy in the range of 0–5 J for a single pulse and an adjustable pulse repetition in the 1–5 Hz range.

The experimental target irradiated by the high-energy laser consists of two parts, one is a superconducting block of YBCO material, and the other, as a load shell, is a commonly used spacecraft aluminum material. The superconducting block is embedded in the center of the aluminum shell. In order to more easily embed the superconductor, we cut off the upper and lower parts of the sphere with two parallel planes symmetric about the center of the sphere, as shown in Fig. 3. Before the laser irradiation, the emitted beacon light is aligned with the center of the target, which guarantees that the laser pulses are aimed at the center of the target. The pinning effect can ensure that the target does not rotate about any axis on the horizontal plane, and the spin angular velocity produced around the vertical axes is very small and can be ignored, so the laser interaction area remains substantially unchanged.

The impulse coupling effect experiment of multi-pulse laser irradiation of the aluminum target includes three processes, in order: creating a low-temperature and low-pressure vacuum environment by air pumping and system cooling; making the target levitate at a set height to create

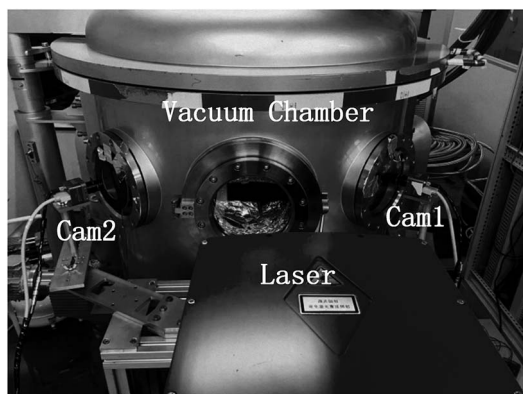


Fig. 2. Photo of the experimental devices.

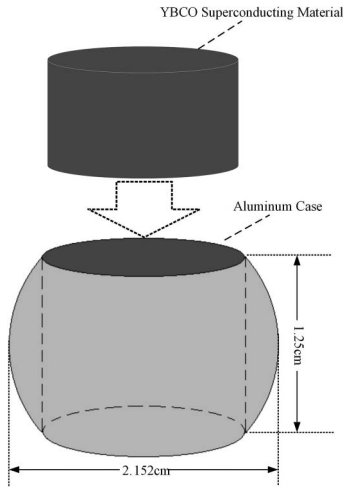


Fig. 3. Target design.

a weightless environment; performing the experiment of laser irradiation on the target and recording the displacement data. The laser parameters are shown in Table 1.

Figure 4 shows the pictures of two cameras capturing the suspending target image. Cameras with a capturing frequency of 50 Hz record the data of approximately 1500 displacements of the suspending target during more than 30 s of pulsed laser irradiation. The displacement versus time curve obtained through the measurement system is shown in Fig. 5. Regardless of the influence between

**Table 1.** Laser Parameters

Parameter	Value
Wavelength	1064 nm
Pulse width	10 ns
Beam diameter	1.2 cm
Energy of single pulse	4.53 J
Pulse reputation frequency	1 Hz

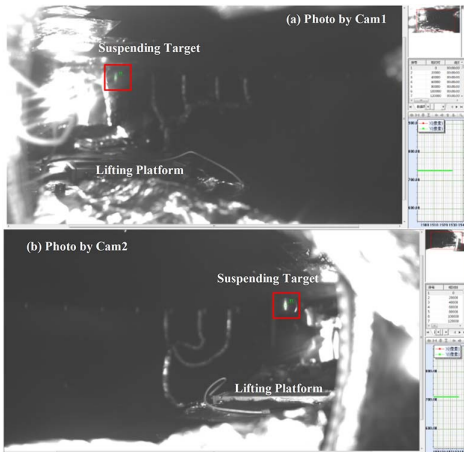


Fig. 4. Track the suspending target.

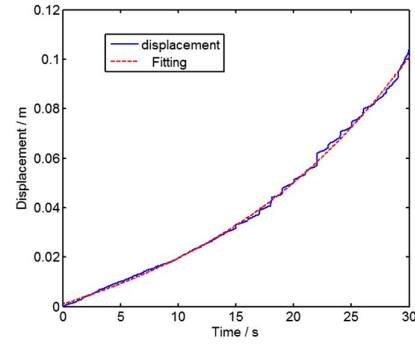


Fig. 5. Curve of displacement with time.

the pulses, the target velocity increases linearly with the number of pulses. Under ideal conditions, the quadratic polynomial fitting relationship is satisfied. However, the actual situation is that the previous pulses will affect the following pulses action, and the cubic polynomial fitting is more suitable for the actual situation. Using the least-squares method, the cubic polynomial is chosen to fit the displacement-time curve. The fitting cubic polynomial is

$$y = 1.39 \times 10^{-6}x^3 + 1.79 \times 10^{-5}x^2 + 1.55 \times 10^{-3}x + 9.84 \times 10^{-4}.$$

Then we obtain the curve of the speed variation with the number of pulses in which the interval time between two pulses is 1 s, as shown in Fig. 6. Using Eq. (1), it also demonstrates the theoretical calculated result<sup>[23]</sup> of the target speed increasement after the first single-pulse laser irradiation. The theoretical value is consistent with the experiment results.

Reference [23] presents a theoretical calculation method for the recoil impulse of a 3D-surface target irradiated by a single-pulse laser,

$$m\Delta v = \iint_S C_m F_{\text{inc}} (\mathbf{e}_{\text{inc}} \cdot \mathbf{n}) \mathbf{n} dA, \quad (1)$$

where  $m$  is the mass of the debris,  $\Delta v$  is the increment of speed obtained by the debris,  $S$  is the integral part of the laser irradiation on the debris surface,  $F_{\text{inc}}$  is the laser

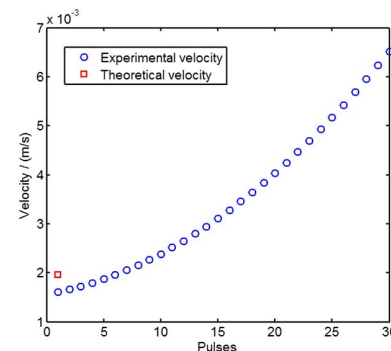


Fig. 6. Curve of velocity with the number of pulses.

power density onto the debris,  $\mathbf{e}_{\text{inc}}$  is the unit direction vector of the incident laser, and  $\mathbf{n}$  is the unit outward-normal vector of the surface differential area  $dA$ . The shape parameters of the target in Fig. 3 and the laser parameters are substituted into Eq. (1), with which we obtain the theoretical calculation value of the recoil impulse of the single-pulse action under the experimental conditions. The theoretical calculation value is the calculation result of the single-pulse coupling, and the influence between two adjacent pulses is not considered, so it has only one result and can only be compared with the first pulse coupling value in our multi-pulse coupling experiment. Comparing the theoretical calculation value with the first pulse coupling value of the multi-pulse experiment, the correctness of the experimental results can be verified to a certain extent.  $C_m$  is the impulse coupling coefficient for quantitatively describing the magnitude of the impulse obtained by consuming unit laser energy<sup>[22]</sup>,

$$C_m = \frac{m\Delta v}{E_{\text{inc}}}, \quad (2)$$

where  $E_{\text{inc}}$  is the incident energy of pulsed laser. Phipps *et al.* have collected experimental data of various wavelengths and pulse widths<sup>[24]</sup>. Assuming the laser energy can completely ionize the target surface<sup>[25]</sup>, they obtained calibration formulas for the impulse coupling coefficient of laser ablating aluminum materials,

$$C_m = 5.56(I\lambda\sqrt{\tau})^{-0.301}, \quad (3)$$

where  $I = F_{\text{inc}}$ ,  $\lambda$  is the laser wavelength, and  $\tau$  is the laser pulse width.

If the recoil impulse of the multi-pulse laser irradiation on the target is a simple linear superposition of the results after every single-pulse action, the displacement over time curve is shown as the red curve in Fig. 7. Obviously, its result is much greater than the experimentally measured displacement. Figure 7 indicates that the multi-pulse impulse coupling effect has its own specific mechanism of action, possibly the interaction between adjacent pulses exiting, so we cannot directly accumulate the results of

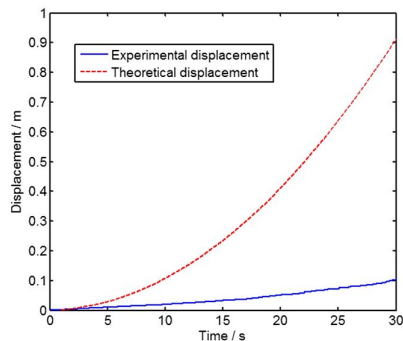


Fig. 7. Comparison between the direct accumulated results of every single-pulse action and the experimental result.

every single-pulse laser coupling with the target as the multi-pulse action.

In order to better study the impulse coupling effect of multi-pulse laser irradiation on space debris, analogous to the method of Eq. (2), the incident laser energy is expressed by the product of the number of pulses and the energy of the single pulse and we call it a multi-pulse impulse coupling coefficient to distinguish from Eq. (2). We must notice that they are essentially identical and it is easy to analyze the effect of the introduction of the number of pulses on the multi-pulse action.

$$C_m = \frac{m\Delta v}{nE_{\text{inc}}}, \quad (4)$$

where  $\Delta v$  is the total speed increment of the target,  $n$  is the number of laser pulses, and  $E_{\text{inc}}$  is the single-pulse energy. The trend of the multi-pulse impulse coupling coefficient changing with the number of pulses is shown in Fig. 8, and also the theoretical calculated result of the impulse coupling coefficient after the first pulse laser irradiation is shown. The reason why there is only one theoretical value is the same as in Fig. 6.

The theoretically calculated values of the velocity increment and the impulse coupling coefficient of the first single-pulse laser irradiation on the target in Fig. 6 and Fig. 8 are slightly larger than the experimental values. It is considered that the laser pulses have a period of air as a medium in the transmission path and must pass through the glass lens into the chamber, so there is laser energy loss, inevitably. Second, the direction of laser emission is not completely horizontal, which may generate an impulse component in the vertical direction for the aluminum target. For these two reasons, the experimental values are smaller than the theoretical values.

Figure 8 shows that the multi-pulse impulse coupling coefficient decreases with the increase of the number of pulses, and finally tends to be stable as the decrease becomes smaller and smaller. For the possible reasons, the temperature rise of the target after the previous pulses action, resulting in an increase in the amount of plasma generated, increases the absorption of the following incident laser energy, which causes the laser energy actually

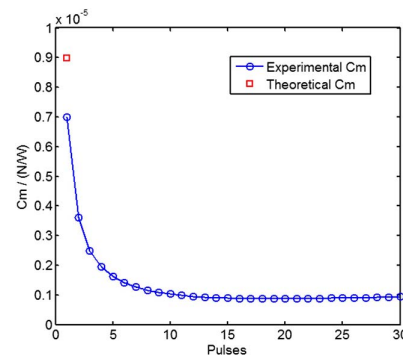


Fig. 8. Trend of the multi-pulse impulse coupling coefficient changing with the number of pulses.

coupling with the target to be reduced. When the amount of plasma generated by subsequent pulses remains relatively stable, the pulse energy coupled with the target also remains stable, so the multi-pulse impulse coupling coefficient will eventually stabilize at a certain level.

It is worth noting that in our experiment, during the first 30 pulses of the laser irradiation on the aluminum target, it is ensured that the aluminum target has a good suspension stability in the vertical direction, but after that, with the following pulses, the aluminum target gradually loses suspension stability, and ultimately is unable to continue suspension. It is an increase in temperature that causes the target to lose the condition that satisfies the pinning effect. There are two main reasons for the temperature rise. First, we used a contact temperature sensor (thermistor) to measure the temperature under continuous pulse action. The laser is set to the parameters corresponding to the experimental laser, and after 30 pulses action, the temperature of the target rose from 294.75 K to 297.82 K. Second, external heat radiation is also an important cause of the target temperature rise. In the experimental verification, even if the laser does not work, the suspending target will eventually fall. The stabilization time is maintained between 20 min and 30 min, and the laser action will accelerate its temperature rise effect.

In summary, this Letter shows the principle of the pinning effect to design a set of experimental systems that can realize a recoil impulse measurement after multi-pulse laser irradiation on space debris with a multi-degree of freedom and without contact damping. Using aluminum as the experimental target, the experiment of the impulse coupling effect of the multi-pulse laser irradiation on space debris was performed and relevant theoretical analysis was carried out. The experimental results demonstrate that the multi-pulse impulse coupling effect is not the direct accumulation of the results of every single-pulse laser coupling with the target, and the multi-pulse impulse coupling coefficient decreases with the increase of the number of pulses, but will eventually stabilize at a certain value. More importantly, it can guide us to calculate the recoil impulse of multi-pulse coupling. The experimental conditions are out of the atmospheric influence, so it is adapted to the space-based laser for debris removal and could provide some reference for the research of the removal process.

We would like to thank the Institute of Electrical Engineering, Chinese Academy of Sciences, Beijing

Institute of Spacecraft Environment Engineering, National University of Defense Technology, and Beijing Information Science and Technology University for providing technical support in our experiment.

## References

1. L. T. Deluca, F. Bernelli, F. Maggi, P. Tadini, C. Pardini, L. Anselmo, M. Grassi, D. Pavarin, A. Francesconi, F. Branz, S. Chiesa, N. Viola, C. Bonnal, V. Trushlyakov, and I. Belokonov, *Acta Astronaut.* **91**, 20 (2013).
2. C. Bonnal, J. M. Ruault, and M. C. Desjean, *Acta Astronaut.* **85**, 51 (2013).
3. V. Braun, A. Lüpken, S. Flegel, J. Gelhaus, M. Mockel, C. Keschull, C. Wiedemann, and P. Vorsmann, *Adv. Space Res.* **51**, 1638 (2013).
4. M. M. Castronuovo, *Acta Astronaut.* **69**, 848 (2011).
5. F. Covello, *Adv. Space Res.* **50**, 918 (2012).
6. D. K. Monroe, *Proc. SPIE* **2121**, 276 (1994).
7. M. Cho, *J. Spacecr. Rockets* **31**, 920 (1994).
8. C. R. Phipps and J. P. Reilly, *Proc. SPIE* **3092**, 728 (1997).
9. W. O. Schall, *Proc. SPIE* **3343**, 564 (1998).
10. W. L. Bohn, *Proc. SPIE* **3612**, 79 (1999).
11. C. Phipps and M. Lander, in *AIP Conference Proceedings, American Institute of Physics* (2011), p. 339.
12. W. O. Schall, *Proc. SPIE* **3574**, 426 (1998).
13. J. W. Campbell and C. R. Taylor, *Proc. SPIE*, **3343**, 583 (1998).
14. J. Liu, L. Ge, L. Feng, H. Jiang, H. Su, T. Zhou, J. Wang, Q. Gao, and J. Li, *Chin. Opt. Lett.* **14**, 051404 (2016).
15. W. O. Schall, *J. Spacecr. Rockets* **39**, 81 (2002).
16. J. T. Early, C. Bibeau, and C. R. Phipps, *AIP Conf. Proc.* **702**, 190 (2004).
17. B. Esmiller and C. Jacqueland, *AIP Conf. Proc.* **1402**, 347 (2011).
18. C. R. Phipps, K. L. Baker, S. B. Libby, D. A. Liedahl, S. S. Olivier, L. D. Pleasance, A. Rubenchik, J. E. Trebes, E. V. George, B. Marcovici, J. P. Reilly, and M. T. Valley, *AIP Conf. Proc.* **1464**, 468 (2012).
19. Z. Liu, Y. Zhang, J. Ding, S. Sun, and B. Hu, *Chin. Opt. Lett.* **15**, 121401 (2017).
20. W. L. Bohn, *AIP Conf. Proc.* **1464**, 442 (2012).
21. T. Ebisuzaki, M. N. Quinn, S. Wada, L. W. Piotrowski, Y. Takizawa, M. Casollino, P. Gorodetzky, E. Parizot, T. Tajima, R. Souldard, and G. Mourou, *Acta Astronaut.* **112**, 102 (2015).
22. C. Phipps, M. Birkan, W. Bohn, H. A. Eckel, H. Horisawa, T. Lippert, M. Michaelis, Y. Rezunkov, A. Sasoh, W. Schall, S. Scharring, and J. Sinko, *J. Propul. Power* **26**, 609 (2010).
23. C. Wang, Y. Zhang, and K. Wang, *Proc. SPIE* **10152**, 101520E (2016).
24. C. R. Phipps, G. K. Anderson, L. C. Haynes, R. F. Harrison, and T. P. Turner, *J. Appl. Phys.* **64**, 1083 (1988).
25. H. Chang, X. Jin, M. Wen, J. Ye, and N. Li, *High Power Laser Part. Beams* **25**, 1110 (2013).